Received: 17 December 2019 | Revised: 3 June 2020 | Accepted: 16 June 2020

DOI: 10.1002/bit.27463

ARTICLE

BIOTECHNOLOGY AND BIOENGINEERING WILEY

Dynamic flux balance analysis of biomass and lipid production by Antarctic thraustochytrid *Oblongichytrium* sp. RT2316-13

Carolina Shene[1] | Paris Paredes[1] | Liset Flores[1] | Allison Leyton[1] | Juan A. Asenjo[2] | Yusuf Chisti[3]

[1]Department of Chemical Engineering, Center of Food Biotechnology and Bioseparations, BIOREN, and Centre of Biotechnology and Bioengineering (CeBiB), Universidad de La Frontera, Temuco, Chile

[2]Department of Chemical Engineering and Biotechnology, Centre for Biotechnology and Bioengineering (CeBiB), Universidad de Chile, Santiago, Chile

[3]School of Engineering, Massey University, Palmerston North, New Zealand

Correspondence
Carolina Shene, Department of Chemical Engineering, Center of Food Biotechnology and Bioseparations, BIOREN, and Centre of Biotechnology and Bioengineering (CeBiB), Universidad de La Frontera, Av. Francisco Salazar 01145, Temuco, Chile.
Email: carolina.shene@ufrontera.cl

Abstract

Production of biomass and lipids in batch cultures of the Antarctic thraustochytrid *Oblongichytrium* sp. RT2316-13, is reported. The microorganism proved capable of producing nearly 67% docosahexaenoic acid (DHA) and 15% eicosapentaenoic acid (EPA) in its total lipid fraction. Biomass with a maximum total lipid content of 33.5% (wt/wt) could be produced at 15°C in batch culture using a medium containing glucose (20 g/L), yeast extract (10.5 g/L), and other minor components. A lower culture temperature (5°C) reduced biomass and lipid productivities compared to culture at 15°C, but enhanced the DHA and EPA content of the lipids by 6.4- and 3.3-fold, respectively. Both a simple minimally structured mathematical model and a more complex genome-scale metabolic model (GEM) allowed the fermentation profiles in batch cultures to be satisfactorily simulated, but the GEM provided much greater insight in the biochemical and physiological phenomena underlying the observed behavior. Unlike the simpler model, the GEM could be interrogated for the possible effects of various external factors such as oxygen supply, on the expected outcomes. In silico predictions of oxygen effects were consistent with literature observations for DHA producing thraustochytrids.

KEYWORDS

docosahexaenoic acid, flux balance analysis, genome-scale metabolic model, lipids, *Oblongichytrium* sp., thraustochytrids

1 | INTRODUCTION

Thraustochytrids are heterotrophic marine biflagellate single-celled eukaryotes, or protists (Gupta, Barrow, & Puri, 2012; Marchan et al., 2018; Singh, Liu, Li, & Wang, 2014). Some thraustochytrids are known to produce large quantities of lipids especially rich in polyunsaturated fatty acids (PUFAs), particularly docosahexaenoic acid (DHA, C22:6n3; Yaguchi, Tanaka, Yokochi, Nakahara, & Higashihara, 1997) and eicosapentaenoic acid (EPA, C20:5n3).

DHA and EPA are nutritionally important fatty acids with different physiological and metabolic roles in humans. EPA is linked to cardiovascular health, regulation of immunity and inflammation, whereas DHA is mostly associated with brain and the nervous system (Weiser, Butt, & Mohajeri, 2016; Winwood, 2013). Although both DHA and EPA can be produced in the human body from the α-linolenic acid, production rates are so low (Brenna, 2002) that consumption of DHA and EPA in the diet provides significant health benefits (Kuratko & Salem, 2013; Linko & Hayakawa, 1996; Sun et al., 2018). Certain marine fish and fish oil are natural sources of EPA and DHA (Pike & Jackson, 2010), but most diets are deficient in these nutrients (Kuratko & Salem, 2013). DHA-rich oils are commercially being produced by several companies using thraustochytrids such as *Schizochytrium* sp. and *Ulkenia* sp. (Kuratko & Salem, 2013; Marchan et al., 2018). Significantly, oils produced in these thraustochytrids have been recognized as safe by competent authorities in the United States and the European Union, for inclusion in human and animal diets (Kuratko & Salem, 2013; Marchan et al., 2018). In thraustochytrids PUFA are found in membrane and

storage (triacylglycerols, tag) lipids at levels that depend on culture conditions (Fan, Jiang, Faan, & Chen, 2007; Okuyama, Orikasa, & Nishida, 2007).

The effects of various external factors on the synthesis of metabolites of interest can be simulated using a genome-scale metabolic model (GEM; Santos, Boele, & Teusink, 2011). Flux balance analysis (FBA) is widely used to analyze the flux of metabolites through the metabolic network of a GEM (Orth, Thiele, & Palsson, 2010). FBA uses linear programming (LP) to maximize an objective function, such as the specific growth rate or the rate of product synthesis, among others (Orth et al., 2010). Because of inherent redundancies in a metabolic network, the same objective function can be obtained for alternate optimal solutions (flux distributions). These may be identified by flux variability analysis (FVA; Mahadevan & Schilling, 2003). FBA has been employed to optimize the specific growth rate and the lipid production rate in the microalga *Chlorella vulgaris* using measured exchange fluxes of the metabolites (Parichehreh, Gheshlaghi, Mahdavia, & Elkamel, 2019). Similarly, FBA has been used to examine changes in intracellular flux distribution in the green microalga *Chlamydomonas reinhardtii* cultured in the presence of acetate (Chapman, Paget, Johnson, & Schwartz, 2015). The effect of light/dark cycles on lipid accumulation by *C. reinhardtii* have been studied using FBA (Shene, Asenjo, & Chisti, 2018). Mass balance equations and FBA results can be used to simulate the dynamic behavior of a cell assuming that the intracellular steady state is rapidly established in response to changes in the extracellular environment. This extension of FBA is known as the dynamic FBA.

This study reports on biomass and lipid production in batch culture of a newly isolated Antarctic thraustochytrid *Oblongichytrium* sp. RT2316-13 (Shene et al., 2019), with a particular focus on synthesis of DHA and EPA. A GEM was used to interpret experimental observations. Furthermore, using FBA and FVA, the GEM was interrogated for the effects of oxygen availability on production of DHA under various scenarios, as discussed.

2 | MATERIALS AND METHODS

2.1 | Microorganism and inoculum preparation

Oblongichytrium sp. RT2316-13 was used. Details of isolation and identification of this marine microorganism were previously published (Shene et al., 2019). The stock cultures were kept frozen at −80°C in 50% glycerol (vol/vol). The inoculum (1 ml of a thawed stock culture) was grown aseptically in an Erlenmeyer flask (250 ml) containing 100 ml of a sterile medium of the following composition (g/L): glucose (Merck, Darmstadt, Germany) 20, yeast extract (BBL™, Becton, Dickinson and Co., Sparks, MD) 6, and monosodium glutamate (Merck) 0.6, in diluted (50% vol/vol) artificial seawater (ASW; Quilodrán, Hinzpeter, Hormazabal, Quiroz, & Shene, 2010). Trace elements and vitamins were added to the medium (Shene et al., 2013). The flask was incubated (15°C) on an orbital shaker (150 rpm) for 5 days.

2.2 | Biomass growth and lipid production

A circumscribed central composite design of experiments (11 experiments, 3 replicates at the central point of the experimental design space) was used to assess the effects of the initial concentration of glucose (*g*) and initial glucose to yeast extract mass ratio (*g/y*) on biomass production and lipid content of the biomass. The coded levels of the factors (0.0, ±1.0, and ±1.41) and the actual values of the concentrations are shown in Table 1. The medium composition that resulted in a biomass sample with the highest lipid content, was used to grow the microorganism at 5°C to determine this effect on lipid synthesis and fatty acid composition of the total lipids.

Each of the runs was started with 20 identical Erlenmeyer flasks inoculated with 5 ml. Except for the noted factors, all the other media components and culture conditions were identical at the levels specified in the previous section. For each run, two flasks were withdrawn every 24 hr; the biomass was recovered by centrifugation (6,000*g*, 4°C, 10 min), washed with distilled water, lyophilized, weighed and stored at −20°C for lipid analysis. The supernatant, was filtered (0.2 μm PTFE membrane) and frozen (−20°C) for further analysis.

2.3 | Measurements of amino acids and glucose

Residual glucose concentration was measured by HPLC (Waters Inc., Milford, MA) using an Aminex HPX-87H column (300 mm length × 7.8 mm internal diameter; Bio-Rad Laboratories Inc., Hercules, CA) kept at 65°C. The mobile phase was sulfuric acid (5 mM) at a flow rate of 0.6 ml/min. A refractive index detector (Waters Inc.) was used. Standard solutions of glucose were used to make a calibration curve.

The total amino acids concentration in the supernatant was determined spectrophotometrically. Thus, a supernatant sample (100 μl) was mixed with 1 ml of the *o*-phthalaldehyde (OPA) reagent (5 mg OPA dissolved in 100 μl of pure ethanol, 5 μl of β-2-mercaptoethanol and 10 ml of 50 mM carbonate buffer, pH 10.5) and the absorbance at 340 nm was measured exactly 2 min after mixing (Bertrand-Harb, Nicolas, Dalgalarraondo, & Chobert, 1993). The blank was made exactly as described, but by replacing the sample with 50% vol/vol ASW. Standard solutions of L-lysine (Sigma, St Louis, MO) in diluted ASW were used to make a calibration curve.

2.4 | Measurements of lipid content of biomass and fatty acid composition of lipid

Total lipids in the freeze-dried biomass (50 mg) were extracted and methylated as described previously (Shene et al., 2019). Fatty acid composition of the methylated lipid extract was determined using a gas chromatograph (GC-2010 Plus; Shimadzu, Kyoto, Japan; Shene et al., 2013).

TABLE 1 Effect of the initial glucose concentration (*g*) and the glucose to yeast extract mass ratio (*g*/*y*; *y*, yeast extract concentration) on the total peak biomass concentration (*X*) and total lipid content (*L*) of RT2316-13 biomass (incubation temperature was 15°C unless specified differently; *t* was the time at peak biomass concentration, (*X*)

Run	g[b]	g/y[b]	g[c] (g/L)	g/y[c] (g/g)	*X* (g/L)	*L* (% wt/wt)	*t* (hr)	Average lipid productivity (mg·L^{-1}·hr^{-1})
1	1	1	30.0	4.3	12.6 ± 1.8	19.2 ± 2.4	192	12.6
2	1	−1	30.0	2.3	14.0 ± 0.1	17.4 ± 1.7	192	12.7
3	−1	1	10.0	4.3	4.3 ± 0.1	23.2 ± 1.0	120	8.3
4	−1	−1	10.0	2.3	5.3 ± 0.2	24.2 ± 0.9	96	13.4
5	1.41	0	34.1	3.3	16.3 ± 0.3	13.9 ± 1.9	192	11.8
6	−1.41	0	5.9	3.3	3.2 ± 0.5	19.1 ± 0.9	72	8.5
7	0	1.41	20.0	4.7	8.0 ± 0.1	24.0 ± 1.0	192	10.0
8	0	−1.41	20.0	1.9	10.5 ± 0.03	33.5 ± 2.2	120	29.3
9	0	0	20.0	3.3	9.0 ± 0.3	23.1 ± 0.6	120	17.3
10	0	0	20.0	3.3	9.2 ± 0.3	22.9 ± 0.3	120	17.6
11[a]	0	0	20.0	3.3	8.7 ± 0.3	23.2 ± 0.8	144	14.0
11[a]	0	0	20.0	3.3	8.0 ± 0.3	20.6 ± 1.0	120	13.7
8[d]	0	−1.41	20.0	1.9	10.1 ± 0.0	15.2 ± 1.9	504	3.0

[a]The data for run 11 are given at 144 hr (the time for peak biomass concentration) and at 120 hr. The 120 hr data allow comparison with the replicate runs 9 and 10 on an identical basis.
[b]Coded values of factors: $g^{¥} = 0.1 \times g^{*} - 2$; $g/y^{¥} = g/y^{*} - 3.33$.
[c]Actual values of factors: $g^{*} = 10 \times (g^{¥} + 2)$; $g/y^{*} = g/y^{¥} + 3.33$.
[d]Culture experiment carried out at 5°C for 24 days.

2.5 | Kinetics of biomass growth, lipid production, and uptake of the substrates

Mass balance equations in terms of the lipid-free biomass concentration (*x*), the total lipids concentration (*l*), glucose concentration (*g*), and total amino acids concentration (*a*) in a batch culture could be written as follows:

$$\frac{1}{x}\frac{da}{dt} = -r_{ta} = -k_1 a, \tag{1}$$

$$\frac{1}{x}\frac{dg}{dt} = -r_g = -k_2 g, \tag{2}$$

$$\frac{1}{x}\frac{dx}{dt} = k_3 r_{ta}, \tag{3}$$

$$\frac{1}{x}\frac{dl}{dt} = k_4 r_g. \tag{4}$$

In the above equations, *t* was time, r_{ta} was the specific consumption rate of total amino acids, r_g was specific consumption rate of glucose, and k_{1-4} were kinetic constants. For each experimental run in Table 1, the kinetic parameters k_{1-4} were determined as the fitted values that minimized the total error calculated as follows:

$$\text{Error} = \sqrt{\frac{1}{n}\sum_{i=1}^{n}(p_{cal} - p_{exp})^2}, \tag{5}$$

where *n* was the number of measurements, p_{cal} was the calculated value of the variables (i.e., *x*, *a*, *g*, *l*) and p_{exp} was the actual experimentally measured value of the variable. The best fit values of the parameters k_{1-4} were computed using MATLAB R2017b (MathWorks Inc., Natick, MA).

2.6 | Genome-scale metabolic model of growth and lipid synthesis by RT2316-13

The GEM of *Schizochytrium limacinum* SR21 (Ye et al., 2015; 1,386 intracellular reactions and 1,659 metabolites) was modified for the strain RT2316-13. The rationale for this was the close relationships among strains of the genera *Oblongichytrium*, *Schizochytrium*, and *Aurantiochytrium*: microorganisms of these genera were all originally placed in *Schizochytrium* until recent emendations (Yokoyama & Honda, 2007) formed two additional genera. The modified model comprised of equations for the neutral lipid-free biomass (11 macro components plus cholesteryl-β-D-glucoside; Table S1) and 1,351 intracellular reactions relating to 1,453 metabolites distributed between the cytosol and mitochondria; 220 previously unused reactions relating to metabolism of amino acids, carbohydrates, and lipids, other metabolisms and reactions for the biomass macro components (Table S1), were added to the model. These reactions (identified in Table S2) enabled: (a) the synthesis of all cell components solely from glucose and amino acids; (b) the synthesis of pyruvate, acetyl-CoA, acetoacetyl-CoA, α-ketoglutarate, suc-CoA, fumarate, and oxaloacetate through metabolism of the 20 available amino acids; and (c) the synthesis of EPA, DHA and arachidonic acid (AA) through the aerobic pathway involving elongases and desaturases, and the polyketide synthase (PKS-like) pathway.

Reaction schemes involved in the synthesis of AA and EPA-DHA through the PKS pathway, were taken from Ujihara, Nagano, Wada, and Mitsuhashi (2014) and Metz et al. (2001), respectively. The actual pathway used for PUFA synthesis was defined by the value assigned to the upper bounds of the respective reactions. KEGG reaction database (https://www.genome.jp/kegg/reaction/; Kanehisa & Goto, 2000) and MetaCyc database (https://metacyc.org/; Caspi et al., 2014) were used to curate the model and fill the gaps.

The mass of 1 mmol of biomass was taken as 1,000 mg in keeping with the norms of FBA (Chan, Cai, Wang, Simons-Senftle, & Maranas, 2017) and the stoichiometric coefficients in the biomass equation corresponded to the mass fraction of each of the macro components (Tables S3 and S4). Fatty acid composition of the different lipids (except tag) and the amino acid composition of the protein fraction, are shown in Tables S5 and S6, respectively. Fatty acid composition of tag was taken from the experimental data of the present study (described in Section 3; Table S7). Because only the fatty acid composition of the different types of lipids was known, lumped equations were used.

All simulations were performed using MATLAB R2017b and the COBRA toolbox (Schellenberger et al., 2011) software packages with Gurobi (version 8.1.1; Gurobi Optimization Inc., Houston, TX) LP/MILP solvers. Matlab codes used in the simulations were deposited in BioModels (Chelliah et al., 2015) database under the assigned identifier MODEL2006010001.

3 | RESULTS AND DISCUSSION

3.1 | Effects of glucose and yeast extract concentrations on production of biomass and lipids

The maximum biomass concentration (16.3 ± 0.3 g/L) was obtained with the conditions of run 5 (g = 34.1 g/L, g/y = 3.3 g/g) whereas the highest lipid content (33.5 ± 2.2%) in the biomass occurred in run 8 (g = 20 g/L, g/y = 1.9 g/g; Table 1). As revealed by the statistical analysis of the data collected at Day 10 (end of the growth experiments; Table S8), glucose concentration positively affected the final dry biomass concentration, whereas the need for yeast extract was reflected in the negative impact of the g/y ratio (i.e., the final dry biomass concentration reduced as the initial yeast extract concentration was reduced; Figure S2a and Equation S1). The lipid content in the 10-day biomass had a highly nonlinear dependence on the g/y ratio in the medium (Figure S2b and Equation S2; ANOVA in Table S9). This nonlinear dependence could be readily explained. In most microorganisms, whenever growth is limited by insufficiency of a nutrient, the available carbon is channeled to the production of storage lipids as growth cannot be sustained if a key nutrient such as sulfur (S), phosphorus (P), or nitrogen (N) is lacking. Lipid content was high at high g/y ratio because N was limiting (y was the only source of N) and carbon (from g and y) was in excess. Lipids also accumulated if g/y was lower than intermediate values (Figure S2b). All cultures with a low g/y entered the stationary phase earlier compared to cultures with intermediate g/y. This was clear for the 12 cultures profiled in Figure S1. When glucose concentration was low and yeast extract concentration was high (i.e., a low g/y ratio), growth was limited by glucose (see Figure S2a), but metabolism of amino acids provided the precursors for the synthesis of lipids.

According to Equation (S2), in a 10-day fermentation, the highest lipid content (30.8% wt/wt) would be obtained with a glucose concentration and the g/y mass ratio equal to 34.1 g/L and 1.9 g/g, respectively. The maximum lipid productivity of RT2316-13 did not exceed 29.3 $mg{\cdot}L^{-1}{\cdot}day^{-1}$ (Table 1). This was comparable to photoautotrophically grown microalgae for which lipid productivity ranged from 11.4 to 82.0 $mg{\cdot}L^{-1}{\cdot}day^{-1}$ (Govindan et al., 2020), although microalgae do display much higher productivities when grown heterotrophically (Bouyam, Choorit, Sirisansaneeyakul, & Chisti, 2017).

3.2 | Effects of incubation temperature on growth and fatty acid composition of total lipids

The conditions of run 8 (Table 1, g = 20 g/L, g/y = 1.9 g/g), that resulted in a high concentration of a biomass with the highest lipid content, were used to assess biomass and lipid production at 5°C. Although the lower incubation temperature slowed cell growth, compared to the results obtained at 15°C (Table 1), the microorganism attained nearly the same final biomass concentration (10.1 g/L; Table 1). The biomass grown at 5°C had a lower total lipids content (15.2% wt/wt; Table 1) compared to the biomass grown at the higher temperature (33.5% wt/wt; Table 1). This was puzzling at first because a reduction in temperature would be expected to reduce both the growth rate and the lipid synthesis rate approximately equally. However, the observed phenomenon had a plausible explanation in terms of the differences in temperature-dependence of the molecular flexibility of the different types of lipids: structural differences in molecules of different types of lipids result in the saturated lipids solidifying, or freezing, at a relatively higher temperature compared to the polyunsaturated lipids. Thus, as the temperature reduced, the synthesis of saturated lipids slowed faster than the synthesis of polyunsaturated lipids, not because of any differences in temperature-dependence of the activity of different enzymes, but because the properties of different classes of lipids were affected differently by temperature. As a consequence, the total rate of lipid synthesis slowed faster than the rate of other metabolic processes, resulting in a lower lipid content in the biomass. As discussed later, this phenomena also explained the observed higher proportion of PUFA in lipids of the biomass grown at the lower temperature.

Growth temperature affected the proportion of PUFA in the total lipid fraction of the biomass. For example, for the lipids recovered from 24-day biomass, the PUFA level was 89.4% (Figure 1a) at 5°C, whereas PUFA content in the lipids of the 10-day biomass was 76.3% at 15°C (Figure 1a). These changes in lipid composition were readily explicable: cold tolerant marine microbes require a high content of PUFA so that the fluidity of the cellular membranes is not

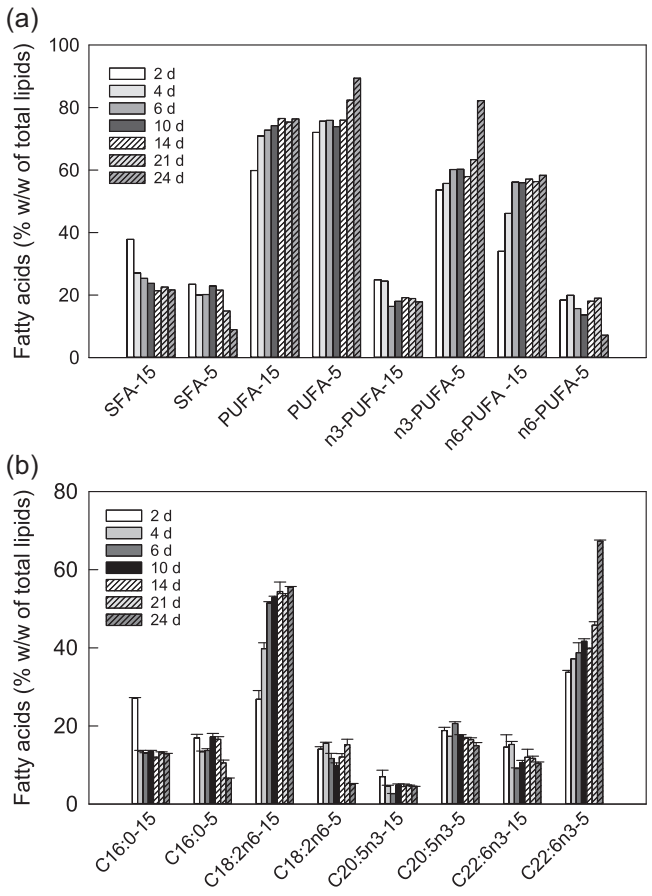

FIGURE 1 Effect of growth temperature (5°C and 15°C) and culture age (d, day) on the content of saturated fatty acids (SFA), total polyunsaturated fatty acids (PUFA), omega-3 (n3) PUFA and omega-6 (n6) PUFA (a) and main fatty acids (b) of the total lipids in RT2316-13. Initial glucose concentration and the glucose to yeast extract mass ratio were 20 g/L and 1.9 g/g, respectively. n3-PUFA-z, omega-3 PUFA at z°C; n6-PUFA-z, omega-6 PUFA at z°C; PUFA-z, total polyunsaturated fatty acids at z°C; SFA-x, total saturated fatty acids at z°C. EPA = C20:5n3; DHA = C22:6n3

lost (Govindan et al., 2020; Valentine & Valentine, 2004). Similar effects of reducing culture temperature on enhanced accumulation of PUFA have been observed in other marine microorganisms such as the diatom *Phaeodactylum tricornutum* (Jiang & Gao, 2004) and the dinoflagellate *Crypthecodinium cohnii* (Jiang & Chen, 2000). From the perspective of production of DHA and EPA, the lipid produced at 5°C was much richer: for example, on Day 24, the contents of EPA and DHA in the lipid produced at 5°C were nearly 3- and 6.4-fold higher, respectively, than in the lipid produced at 15°C (Figure 1b). Lipid concentration in the experiment carried out at 15°C for 10 days (3.5 ± 0.2 g/L) was 2.2-fold higher than in the experiment at 5°C after 24 days. Considering the EPA and DHA content of the total fatty acids (Figure 1b), their concentrations were 0.24 ± 0.03 and 1.07 ± 0.13 g/L, respectively, in the experiment carried out at the lower temperature. These value were 1.5- and 2.9-fold higher than the concentrations of EPA and DHA obtained in the experiment performed at 15°C.

3.3 | Kinetics of growth

A simple mathematical model (Equations 1–4) was used to derive the relationships for the specific consumption rates of glucose and total amino acids that could be used to predict the growth of the lipid-free biomass and production of total lipids. The model assumed that the synthesis of the lipid-free biomass had a first-order dependence on the concentration of total amino acids. This assumption was based on the observed high content of protein (48.65%) in the biomass (Table S3) and the fact that amino acids can provide carbon and nitrogen that are both necessary for growth. The model further assumed that the synthesis rate of total lipids depended on the glucose uptake rate (Equation 4) that was a function of glucose concentration (Equation 2). Glucose provides only carbon and therefore can support the synthesis of neutral lipids that generally lack nitrogen in their molecules. The best fit values of the parameters in the kinetic relationships (k_{1-4}), for each experimental run shown in Table 1 and the error (Equation 5), are provided in Table S10. As shown in Figure S1, the model fitted the culture concentration profiles for all the runs. Therefore, the simple model (Equations 1–4) was adequate for the intended purpose of predicting the biomass concentration, the lipid content of the biomass, consumption of glucose and consumption of total amino acids. A unified model with the same set of values of k_{1-4} for all the cultures in Figure S1 could not be obtained, possibly because the initial concentrations of nutrients in the different runs varied over a broad range (nearly 6-fold variation in g and a 2.5-fold variation in g/y).

3.4 | Dynamic FBA for the prediction of growth and tag synthesis

To simulate the synthesis and accumulation of tag, this macro component was not included in the biomass equation, and was considered a secondary product of lipid-free biomass. The fatty acid composition of tag was assumed to be the value shown for day 8 in the lipids produced at 5°C (Table S7). Generally, tag are synthesized after cell growth has ceased due to nitrogen limitation if the C-source is abundant. Once growth has ceased, the only model objective function that needs to be maximized is the synthesis of neutral lipids. On the other hand, some neutral lipid are produced simultaneously with growth. In this scenario, a part of the glucose is consumed for growth and maintenance whereas the rest is consumed for lipid synthesis. Therefore, for tag synthesis during cell growth, simulations required information about partitioning of the internalized glucose. To resolve this, a parameter denoted f_{G_bio}, defined as the fraction of the specific consumption rate of glucose (r_g) that was diverted to synthesis of the various macro components of the tag-free biomass, was used.

For a given set of values of the lower bound of the oxygen exchange reaction (r_{O_2}), the specific rate of ATP synthesis for cell maintenance (r_{ATP_m}) and f_{G_bio}, the following procedure was used to compute the concentration profiles using dynamic FBA:

(i) Initial concentrations of glucose (g_0) and total amino acids (a_0, estimated from the composition of the yeast extract; Table S11) were used to compute the specific consumption rates of total amino acids (r_{ta}; Equation 1) and glucose (r_g; Equation 2) using the values of the parameters k_1 and k_2 (Table S10).

(ii) The lower bound of the glucose exchange reaction ($v_{g,lb}$) was fixed at $-r_g \times f_{G\_bio}$. The lower bounds of the exchange reactions of each amino ($r_{a,i}$) acid was estimated from the specific consumption rate of total amino acids (r_{ta}) multiplied by the mass fraction of the amino acid in the total amino acids, and a conversion factor (see note at the bottom of Table S11).

(iii) FBA was used to maximize μ by solving the following LP problem:

$$\begin{aligned} &\max \quad (\mu) \\ &\text{s. t.} \quad S_{m\times n} \times \nu = 0, \\ &-r_g \times f_{G\_bio} \le \nu_g \le 0, \\ &-r_{a,i} \le \nu_{a,i} \le 0 \quad (i = 1, \ldots, 20), \\ &-r_{O_2} \le \nu_{O_2} \le 0, \\ &\nu_{j,lb} \le \nu \le \nu_{j,ub}. \end{aligned} \tag{6}$$

Here S is the stoichiometric matrix, m is the number of metabolites, n is the number of reactions, and v is the reaction rate vector; v_g is the specific rate of glucose consumption, $v_{a,i}$ is the specific consumption rate of amino acid i (i = 1,..., 20), and ν_{O_2} is the specific consumption rate of oxygen. The parameters $v_{j,lb}$ and $v_{j,ub}$ are the lower and upper bounds of each of the other reactions in the stoichiometric matrix.The maximum v_{tag} was obtained by solving:

$$\begin{aligned} &\max(v_{tag}) \\ &s.\ t.\ S \times \nu = 0 \\ &\nu_{bio,lb} = \nu_{bio,ub} = \mu, \\ &-r_g \le \nu_g \le 0 \\ &-r_{a,i} \le \nu_{a,i} \le 0 \quad (i = 1, \ldots, 20), \\ &-r_{O_2} \le \nu_{O_2} \le 0, \\ &\nu_{j,lb} \le \nu \le \nu_{j,ub}. \end{aligned} \tag{7}$$

In solving the above, the lower ($v_{bio,lb}$) and upper ($v_{bio,ub}$) bounds for the flux through the tag-free biomass equation (Table S1) were set to the value of μ determined in the previous step, and the lower bound of the glucose exchange rate was set to $-r_g$.

(iv) The lower and upper bounds for the flux through the tag were fixed as the solution of LP in (7), and the minimum and maximum values for the glucose exchange reaction, and the exchange reactions for each amino acid, were obtained from FVA.

(v) Values of $\nu_{a_i,max}$ and $v_{g,max}$ obtained earlier (step v) were used to compute the change of the concentration of glucose (g) and each amino acids (a_i). As nutrient consumption rates have negative values, the maximum value was the minimum consumption rate that maximized the target objectives. A finite difference approximation of the differential equations corresponding to the mass balances (batch culture) was used:

$$x_{tf}(t + \Delta t) = x_{tf}(t) + \Delta t \times x_{tf}(t) x \mu, \tag{8}$$

$$g(t + \Delta t) = g(t) + \Delta t \times x_{tf}(t) \times \nu_{g,max}, \tag{9}$$

$$tag(t + \Delta t) = tag(t) + \Delta t x x_{tf}(t) x \nu_{tag}, \tag{10}$$

$$a_i(t + \Delta t) = a_i(t) + \Delta t \times x_{tf}(t) \times \nu_{a_i,max}, \tag{11}$$

$$a(t + \Delta t) = \sum_{i=1}^{20} a_i(t + \Delta t). \tag{12}$$

Here Δt was the time step set to 0.5 hr, and x_{tf} was the concentration of the tag-free biomass. Concentration of the lipid-free biomass (x) and total lipids (l) were obtained from the following equations:

$$x(t + \Delta t) = x_{tf}(t + \Delta t) \times (1 - 0.1891), \tag{13}$$

$$l(t + \Delta t) = x_{tf}(t + \Delta t) \times 0.1891 + tag(t + \Delta t), \tag{14}$$

where 0.1891 was the mass fraction of other lipids (polar lipids, free fatty acids, and unsaponifiable matter) in the tag-free biomass (Table S3). The values of the concentration of glucose and total amino acids obtained in Equations (9) and (12), respectively, were used for the next integration step.

A solution for the LP problem in Equation (6) was obtained when glucose, amino acids, and oxygen were consumed at rates that enabled the synthesis of the different biomass components and ATP for maintenance. When the growth curve was simulated, the consumption rate of glucose decreased because its concentration decreased (Equation 2). Depending on the growth conditions, the rate of glucose consumption decreased to a level that was insufficient for ATP synthesis for maintenance (r_{ATP_m}) and the LP problem had no solution. The time at which this occurred depended on the value of the lower bound of the oxygen exchange rate. Considering that the rate of ATP consumption for maintenance could vary from high values during rapid growth to low values under growth limiting conditions (Farmer & Jones, 1976), the final part of the growth curve was simulated assuming r_{ATP_m} equal to 0 mmol·g^{-1} DW·hr^{-1}). The fermentation profiles for this condition (r_{ATP_m} = 0 mmol·g^{-1} DW·hr^{-1}) are shown as dashed lines in Figure 2.

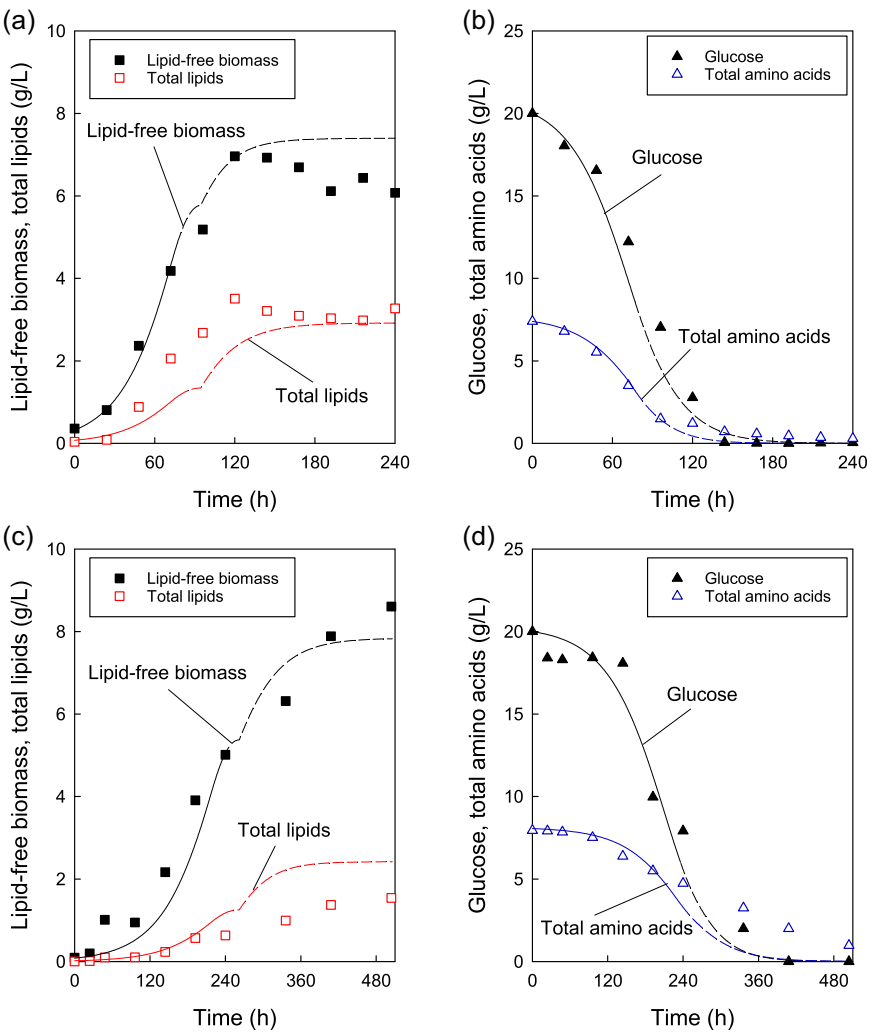

FIGURE 2 Comparison of the experimental data (symbols, run 8 in Table 1) and the predictions of the genome-scale metabolic model (GEM; continuous lines) at (a,b) 15°C and (c,d) 5°C. (a,c) Production of lipid-free biomass and total lipids and (b,d) consumption of glucose and total amino acids. Parameters r_{ATP_m} and f_{G_bio} used in the simulations and the lower bound of the specific oxygen uptake rate were: 6 mmol·g^{-1} DW·hr^{-1}, 1.0 (−), and − 1.25 mmol·g^{-1} DW·hr^{-1}, respectively, in (a, b) and 3 mmol·g^{-1} DW·hr^{-1}, 1.0 (−), and − 0.62 mmol·g^{-1} DW·hr^{-1}, respectively, in (c,d). Dashed lines show the results after r_{ATP_m} was set to 0 mmol·g^{-1} DW·hr^{-1} [Color figure can be viewed at wileyonlinelibrary.com]

In step (ii), the specific consumption rate of each amino acid was taken to depend on the mass fraction of that amino acid in the mixture of amino acids (i.e., yeast extract). In principle, the consumption rate of an amino acid is expected to depend on how much of it is needed for protein synthesis, but microbial proteins generally have similar amino acid compositions. For example, a comparison of the amino acid composition of RT2316-13 protein (Table S6) with the published composition of yeast protein (Peppler, 1965) confirmed that the levels of 12 amino acids in the two proteins did not differ by more than ±1%.

For the conditions of run 8 (Table 1) the values of r_{ATP_m} and f_{G_bio} that allowed total average error (Equation 5) to be reduced to 1.55 g/L, were 6 mmol·g^{-1} DW·hr^{-1} and 1.0 (−), respectively, under an oxygen sufficient condition. Under a moderate oxygen limitation (r_{O_2} = −1.25 mmol·g^{-1} DW·hr^{-1}), the predictions improved (average total error = 0.82 g/L). With these parameters (r_{ATP_m} = 6 mmol·g^{-1} DW·hr^{-1} for t < 94.5 hr; f_{G_bio} = 1.0, and r_{O_2} = −1.25 mmol·g^{-1} DW·hr^{-1}) the specific growth rate decreased from 40.4×10^{-3} to 1×10^{-5} hr^{-1} (not shown) as the concentration of nutrients decreased. Figure 2a,b compare the experimental and simulated concentration profiles (run 8, 15°C) of the lipid-free biomass, total lipids, glucose, and total amino acids. Figure 2c,d compare the experimental data and the model-predicted concentration profiles for run 8 performed at 5°C. Values of r_{ATP_m} and f_{G_bio} were 3.0 mmol·g^{-1} DW·hr^{-1} (for t < 342 hr), and 1.0 (−), respectively, and $r_{O_{2,lb}}$ was fixed at −0.62 mmol·g^{-1} DW·hr^{-1} (average total error = 1.26 g/L). With these parameters, the specific growth rate decreased from 19.6×10^{-3} to 4×10^{-5} hr^{-1} (not shown), as the concentrations of nutrients declined.

3.5 | Effect of the PUFA synthesis pathway on growth and tag synthesis

Some thraustochytrids can produce PUFA using two distinct pathways (Marchan et al., 2018; Metz et al., 2001; Qiu, Hong, & MacKenzie, 2001): the well-known elongase–desaturase pathway (oxygen-dependent), and the anaerobic polyketide synthase-like pathway (PKS). Although both pathways use the same precursors (i.e., acetyl-CoA and NADPH), energy requirements are different (Aasen et al., 2016).

Flux distribution through some of the reactions in the metabolic network (Figure 3) was analyzed for two in silico strains: the aerobic strain (synthesizes DHA and EPA only via the aerobic pathway) and the PKS strain (uses only the PKS-like pathway). Growth conditions were those of run 8°C at 15°C (Table 1). In this experiment the initial consumption rates of glucose and total amino acids were 0.551 and 0.363 mmol·g^{-1} DW·hr^{-1}, respectively. Figure 3 shows the flux through reactions that presented no variability when the oxygen exchange rate was not constrained and when the lower bound of this reaction was set to −0.9 mmol·g^{-1} DW·hr^{-1}. Figure 4 shows the variability range of reactions in Figure 3 for the two in silico strains and the two oxygen uptake conditions. Values for other reactions can be found in Supporting Information (Flux Variability Analysis Shene et al).

Under no oxygen limitation, the two in silico strains grew at the same specific growth rate (0.0612 hr^{-1}); however the in silico PKS strain synthesized tag at a rate 1.12-fold higher than the aerobic strain (0.015 mmol·g^{-1} DW·hr^{-1}). Fluxes through most of the reactions in the upper part of glycolysis and the nonoxidative pentose phosphate pathways showed no variability in the two in silico strains (Figure 3). For the 26 reactions shown in Figure 3 that presented variability under no oxygen limitation, variability range of 13 reactions (related to lipid and amino acid metabolism) was smaller in the aerobic in silico strain (Figure 4b) than in the PKS strain (Figure 4a) because of the lower rate of tag synthesis in the aerobic strain. Both minimum and maximum fluxes of three reactions (NADH-ubiquinone oxidoreductase [EC 7.1.1.2], electron-transferring-flavoprotein dehydrogenase [EC 1.5.5.1], and mitochondrial fumarate hydratase [EC 4.2.1.2]) presented higher values in the aerobic in silico strain than in the PKS strain (Figure 4a,b). Combined, these reactions regenerate FADH2 cofactor generated in the synthesis of 2-methylcrotanoyl-CoA (acyl-CoA dehydrogenase, EC 1.3.99.12). In the aerobic in silico strain the flux through the mitochondrial reaction catalyzed by citramalate synthase was 10-fold higher than in the PKS strain. Citramalate is transformed through several consecutive reactions (in the mitochondria and then in the cytosol) becoming one of the sources to the substrate for the synthesis of 2-methylcrotanoyl-CoA.

Although the in silico aerobic strain synthesized the PUFA containing tag at a specific rate lower than in the PKS strain, it produced NADPH (through the pentose phosphate pathway reactions (glucose-6-phosphate dehydrogenase (EC 1.1.1.49), and phosphogluconate dehydrogenase (EC 1.1.1.44)) at a rate 1.13-fold higher when the r_{O_2} was not constrained. This was attributed to the NADPH-requiring synthesis of structural lipids (Tables S2 and S3), that took place at the same specific rate, but required more of the cofactor as aerobic pathway was being used. The null flux through the reaction catalyzed by the malic enzyme was explained by the low specific rate of tag synthesis (f_{G_bio} = 0.9, 90% of the consumed glucose was used for cell growth). When all the consumed glucose was used for tag synthesis (f_{G_bio} = 0) the flux through this reaction became different from zero (not shown). These results differ from those reported for a *S. limacinum* strain in which the three above mentioned NAPDH sources contributed almost equally to regeneration of the cofactor (Ye et al., 2015).

The high flux variability of the reaction catalyzed by ATP citrate synthase (ATPCS, EC 2.3.3.8; Figure 4a) was indicative of substitutable reactions. Metabolism of leucine, tyrosine, and phenylalanine also contributed to production of acetyl-CoA (Flux Variability Analysis Shene et al. in Supporting Information). One alternate solution was found to produce acetyl-CoA from acetoacetyl-CoA (EC 2.3.1.9). The acetoacetyl-CoA was the final product of lysine metabolism pathway (Flux Variability Analysis Shene et al. in Supporting Information). According to an earlier report, activity of saccharopine dehydrogenase (EC 1.5.1.7; one of the enzymes of the lysine metabolism pathway) was not detected in extracts of *Thraustochytrium aureum* (Paton & Jennings, 1989), a related microorganism, therefore the contribution of this reaction to production of acetyl-CoA was tested. When the lower and upper bounds through this reaction (SSAL(NAD)) were fixed at 0 mmol·g^{-1} DW·hr^{-1}, lysine consumption rate was substantially affected (42% decrease), the specific growth rate decreased (4%), and because of this reduction the specific rate of tag synthesis increased (4%) in the two in silico strains (Flux Variability Analysis Shene et al. in Supporting Information).

Above results showed that the aerobic strain exchanged oxygen at a higher rate than the PKS strain (Figure 4b); thus oxygen limitation (constraining $r_{O_2,lb}$ to a specific value) will have a higher impact on the metabolism of the aerobic strain. The oxygen limiting condition ($r_{O_2,lb}$ = −0.9 mmol·g^{-1} DW·hr^{-1}) had no effect on the specific growth rate of the two in silico strains. In contrast, the specific rate of tag synthesis in the in silico PKS strain was reduced by 47% and in the in silico aerobic strain it was reduced by 91%. This was explained by the reduced rate of ATP synthesis in the mitochondria resulting in a decreased rate of citrate synthesis which in turn reduced the synthesis rate of acetyl-CoA (Figure 3). Only one of the reactions shown in Figure 3 (PKY, pyruvate kinase) presented an important variability in the in silico PKS strain under the oxygen limiting condition (Figure 4c). In the aerobic in silico strain the number of reactions with flux variability was reduced and the exchange of succinate and citrate was promoted (Figure 4d) because they could not be channeled into the synthesis of acetyl-CoA.A high dissolved oxygen concentration has been reported to favor biomass production of *Schizochytrium* (Chi, Liu, Frear, & Chen, 2009; Zhang, Zhao, Lai, Wu, & Chen, 2013) and other thraustochytrids (Aasen et al., 2016; Marchan et al., 2018; Winwood, 2013), but has negatively affected the lipid content of the biomass (Aasen et al., 2016; Chi et al., 2009; Marchan et al., 2018; Zhang et al., 2013).

4 | CONCLUSIONS

For the Antarctic thraustochytrid *Oblongichytrium* sp. at 15°C, maximum biomass concentration (16.3 g/L on Day 8) and lipid content in the biomass (33.5% wt/wt on Day 5) were achieved with different initial glucose concentrations and practically the same yeast extract concentration. The lower incubation temperature (5°C) elevated the EPA and DHA content of the total lipids by at least three-fold compared to lipids produced at 15°C, but this did not compensate for

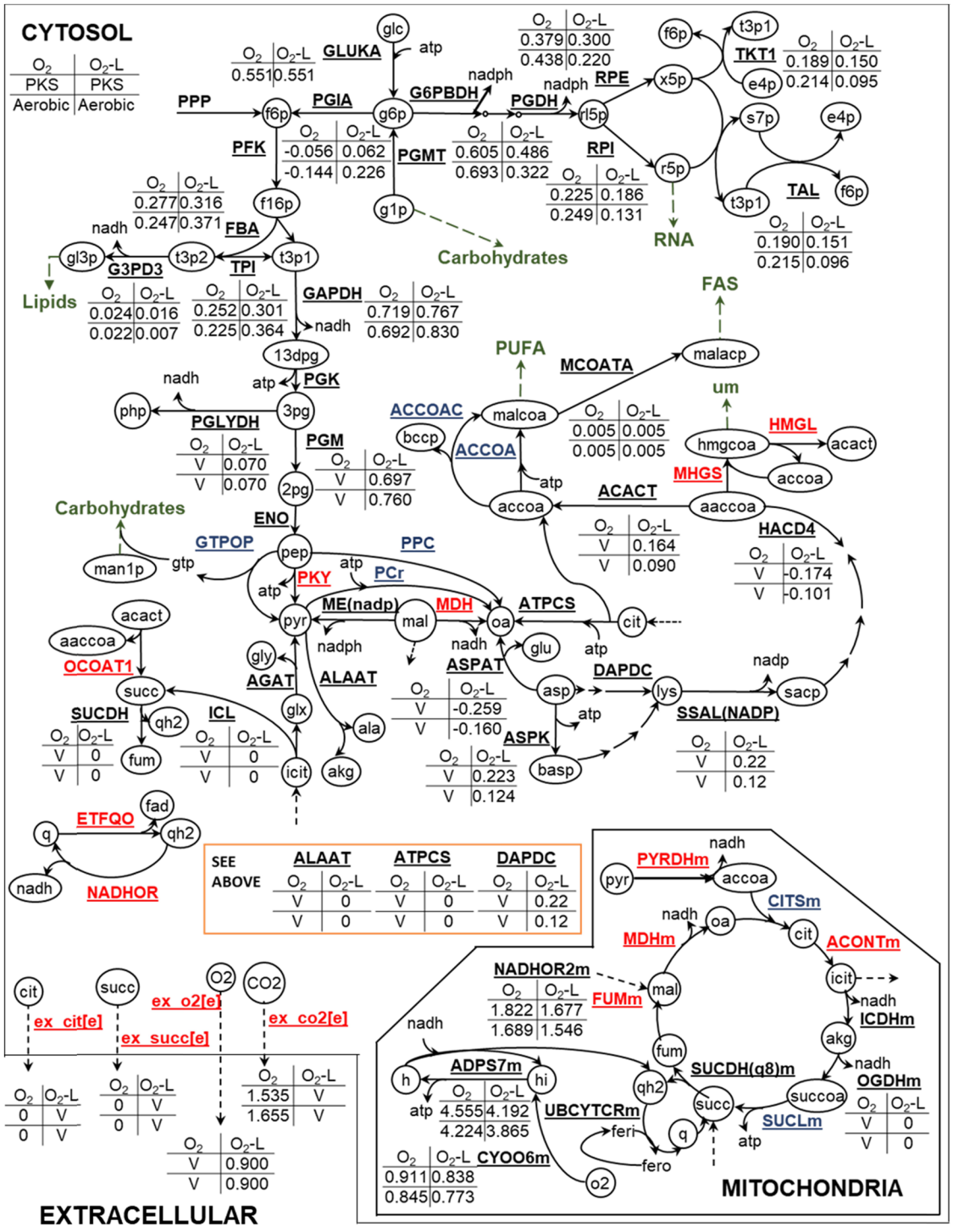

FIGURE 3 Comparison of flux distribution through some of the reactions in the metabolic network. Abbreviated names of the reactions with no flux variability are in black; name of reactions with flux variability are in red; reactions that are part of alternate solutions are in blue. Tables near the reaction names show the flux for the two in silico strains (PKS and aerobic) under oxygen sufficient (O_2) and oxygen limiting (O_2-L) conditions. Oxygen limiting condition was computed with the lower bound of the specific oxygen exchange rate set to −0.9 mmol·g^{-1} DW·hr^{-1}. V denotes that the flux for the specified condition (strain—O_2 condition) presented variability. Variability range for these reactions and those shown in red, is given in Figure 4. The abbreviations are explained in the Excel file "Flux Variability Analysis Shene et al" (Supporting Information) [Color figure can be viewed at wileyonlinelibrary.com]

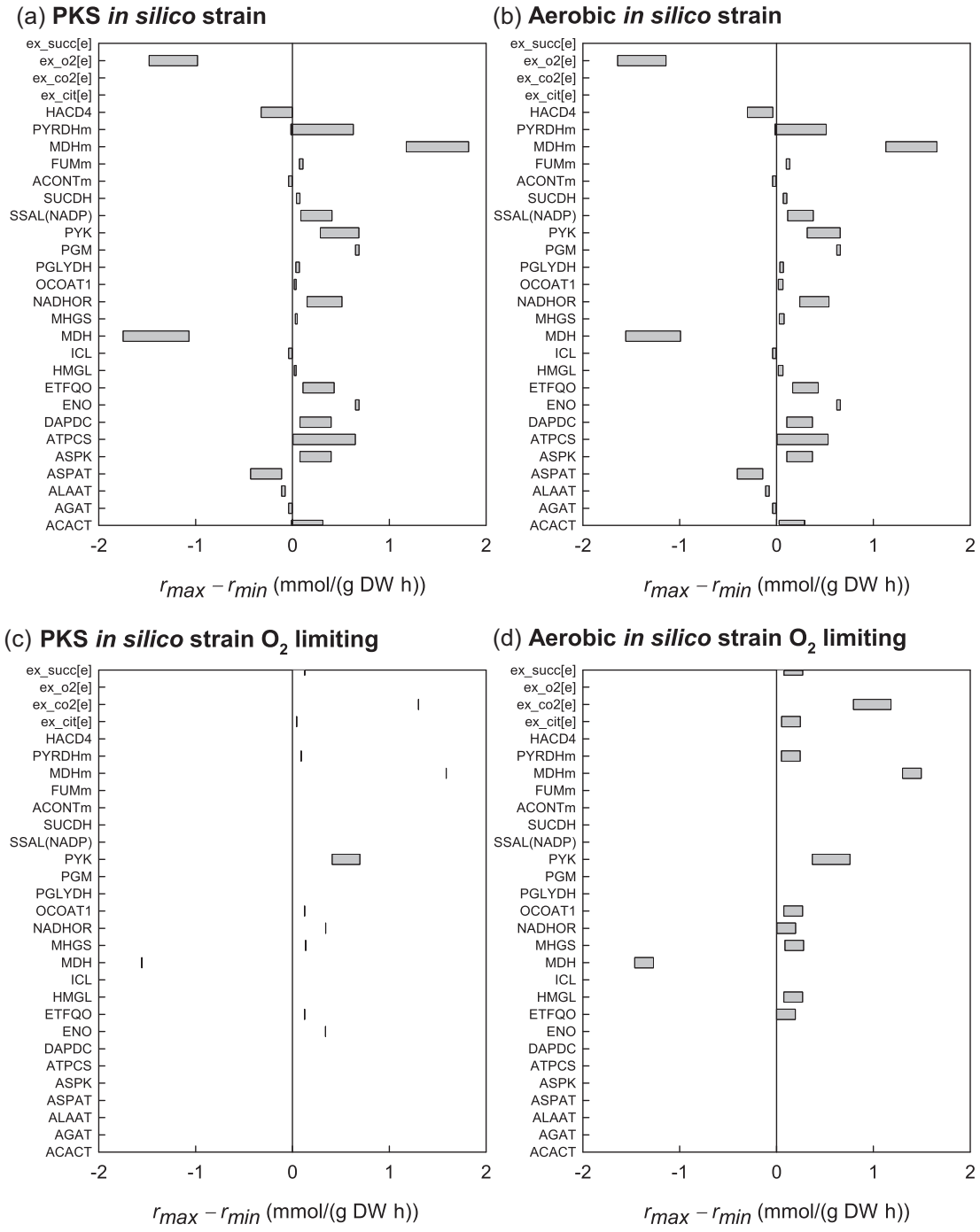

FIGURE 4 Comparison of the flux variability range (maximum rate − minimum rate) through the reactions of the metabolic network shown in Figure 3. Results for the in silico strains that synthesized eicosapentaenoic acid (EPA) and eicosapentaenoic acid (EPA) through the polyketide synthase (PKS) (a,c) and aerobic (b,d) pathways without constraining the specific oxygen exchange rate (a,b) and computed with the lower bound of the specific oxygen exchange rate set to −0.9 mmol·g^{-1} DW·hr^{-1} (c,d). The abbreviations are explained in the Excel file "Flux Variability Analysis Shene et al" (Supporting Information)

the productivity loss that accompanied the reduced incubation temperature.

Dynamic FBA was satisfactorily used to simulate the concentration profiles of biomass and total lipids in the biomass. For this, relationships for the specific consumption rates of the nutrients (glucose and amino acids) were needed. FBA and FVA showed that the effect of oxygen availability on the specific tag synthesis rate depended on the pathway being used for the synthesis of EPA and DHA. The tag synthesis rate decreased less in a PKS strain subjected to oxygen limitation. FBA showed that the metabolism of some amino acids contributed to the tag synthesis rate. These results, combined with data from more sophisticated experiments relating to the fate of

each amino acid, could in the future be used in designing a culture medium for enhancing the rate of tag synthesis.

ACKNOWLEDGMENTS

This study was supported by the following: Instituto Antártico Chileno (INACH) project Inach RT 23-16, Chile; National Fund for Scientific and Technological Development (Fondecyt postdoctoral project No. 3170610), Chile; Dirección de Investigación, Universidad de La Frontera (GAP funding and undergraduate program); and the Centre for Biotechnology and Bioengineering (CeBiB) (Conicyt grant FB-0001).

CONFLICT OF INTERESTS

The authors declare that there are no conflict of interests.

AUTHOR CONTRIBUTIONS

C. S. conceived the research project leading to this publication. P. P., A. L., and L. F. performed the experiments and prepared the initial draft of the manuscript. C. S., J. A., and Y. C. discussed the results and wrote the final manuscript.

ORCID

Carolina Shene http://orcid.org/0000-0003-4646-038X
Allison Leyton http://orcid.org/0000-0002-8665-267X
Juan A. Asenjo https://orcid.org/0000-0002-3475-7664
Yusuf Chisti https://orcid.org/0000-0002-0826-7012

REFERENCES

Aasen, I. M., Ertesvåg, H., Heggeset, T. M. B., Liu, B., Brautaset, T., Vadstein, O., & Ellingsen, T. E. (2016). Thraustochytrids as production organisms for docosahexaenoic acid (DHA), squalene, and carotenoids. *Applied Microbiology and Biotechnology*, *100*, 4309–4321. https://doi.org/10.1007/s00253-016-7498-4

Bertrand-Harb, C., Nicolas, M. G., Dalgalarraondo, M., & Chobert, J. M. (1993). Determination of alkylation degree by three colorimetric methods and amino-acid analysis? A comparative study. *Science des Aliments*, *13*, 577–584.

Bouyam, S., Choorit, W., Sirisansaneeyakul, S., & Chisti, Y. (2017). Heterotrophic production of *Chlorella* sp. TISTR 8990—Biomass growth and composition under various production conditions. *Biotechnology Progress*, *33*, 1589–1600. https://doi.org/10.1002/btpr.2518

Brenna, J. T. (2002). Efficiency of conversion of α-linolenic acid to long chain n-3 fatty acids in man. *Current Opinion in Clinical Nutrition and Metabolic Care*, *5*, 127–132. https://doi.org/10.1097/00075197-200203000-00002

Caspi, R., Altman, T., Billington, R., Dreher, K., Foerster, H., Fulcher, C. A., … Karp, P. D. (2014). The MetaCyc database of metabolic pathways and enzymes and the BioCyc collection of pathway/genome databases. *Nucleic Acids Research*, *40*, D742–D753. https://doi.org/10.1093/nar/gkr1014

Chan, S. H. J., Cai, J., Wang, L., Simons-Senftle, M. N., & Maranas, C. D. (2017). Standardizing biomass reactions and ensuring complete mass balance in genome-scale metabolic models. *Bioinformatics*, *33*, 3603–3609. https://doi.org/10.1093/bioinformatics/btx453

Chapman, S. P., Paget, C. M., Johnson, G. N., & Schwartz, J. M. (2015). Flux balance analysis reveals acetate metabolism modulates cyclic electron flow and alternative glycolytic pathways in *Chlamydomonas reinhardtii*. *Frontiers in Plant Science*, *6*, 474. https://doi.org/10.3389/fpls.2015.00474

Chelliah, V., Juty, N., Ajmera, I., Ali, R., Dumousseau, M., Glont, M., … Laibe, C. (2015). BioModels: Ten-year anniversary. *Nucleic Acids Research*, *43*, D542–D548. https://doi.org/10.1093/nar/gku1181

Chi, Z., Liu, Y., Frear, C., & Chen, S. (2009). Study of a two-stage growth of DHA-producing marine algae *Schizochytrium limacinum* SR21 with shifting dissolved oxygen level. *Applied Microbiology and Biotechnology*, *81*, 1141–1148. https://doi.org/10.1007/s00253-008-1740-7

Fan, K. W., Jiang, Y., Faan, Y. W., & Chen, F. (2007). Lipid characterization of mangrove thraustochytrid-*Schizochytrium mangrovei*. *Journal of Agricultural and Food Chemistry*, *55*, 2906–2910. https://doi.org/10.1021/jf070058y

Farmer, I. S., & Jones, C. W. (1976). The energetics of *Escherichia coli* during aerobic growth in continuous culture. *European Journal of Biochemistry*, *67*, 115–122. https://doi.org/10.1111/j.1432-1033.1976.tb10639.x

Govindan, N., Maniam, G. P., Yusoff, M. M., Rahim, M. H. A., Chatsungnoen, T., Ramaraj, R., & Chisti, Y. (2020). Statistical optimization of lipid production by the diatom *Gyrosigma* sp. grown in industrial wastewater. *Journal of Applied Phycology*, *32*, 375–387. https://doi.org/10.1007/s10811-019-01971-x

Gupta, A., Barrow, C. J., & Puri, M. (2012). Omega-3 biotechnology: Thraustochytrids as a novel source of omega-3 oils. *Biotechnology Advances*, *30*, 1733–1745. https://doi.org/10.1016/j.biotechadv.2012.02.014

Jiang, H., & Gao, K. (2004). Effects of lowering temperature during culture on the production of polyunsaturated fatty acids in the marine diatom *Phaeodactylum tricornutum* (Bacillariophyceae). *Journal of Phycology*, *40*, 651–654. https://doi.org/10.1111/j.1529-8817.2004.03112.x

Jiang, Y., & Chen, F. (2000). Effects of temperature and temperature shift on docosahexaenoic acid production by the marine microalgae *Crypthecodinium cohnii*. *Journal of the American Oil Chemists' Society*, *77*, 613–617. https://doi.org/10.1007/s11746-000-0099-0

Kanehisa, M., & Goto, S. (2000). KEGG: Kyoto Encyclopedia of Genes and Genomes. *Nucleic Acids Research*, *28*, 27–30. https://doi.org/10.1093/nar/28.1.27

Kuratko, C. N., & Salem, N., Jr. (2013). Docosahexaenoic acid from algal oil. *European Journal of Lipid Science and Technology*, *115*, 965–976. https://doi.org/10.1002/ejlt.201300060

Linko, Y.-Y., & Hayakawa, K. (1996). Docosahexaenoic acid: A valuable nutraceutical? *Trends in Food Science and Technology*, *7*, 59–63. https://doi.org/10.1016/0924-2244(96)81329-X

Mahadevan, R., & Schilling, C. H. (2003). The effects of alternate optimal solutions in constraint-based genome-scale metabolic models. *Metabolic Engineering*, *5*, 264–276. https://doi.org/10.1016/j.ymben.2003.09.002

Marchan, L. F., Chang, K. J. L., Nichols, P. D., Mitchell, W. J., Polglase, J. L., & Gutierrez, T. (2018). Taxonomy, ecology and biotechnological applications of thraustochytrids: A review. *Biotechnology Advances*, *36*, 26–46. https://doi.org/10.1016/j.biotechadv.2017.09.003

Metz, J., Roessler, P., Facciotti, D., Levering, C., Dittrich, F., Lassner, M., … Browse, J. (2001). Production of polyunsaturated fatty acids by polyketide synthases in both prokaryotes and eukaryotes. *Science*, *293*, 290–293. https://doi.org/10.1126/science.1059593

Okuyama, H., Orikasa, Y., & Nishida, T. (2007). In vivo conversion of triacylglycerol to docosahexaenoic acid-containing phospholipids in a thraustochytrid-like microorganism, strain 12B. *Biotechnology Letters*, *29*, 1977–1981. https://doi.org/10.1007/s10529-007-9492-5

Orth, J. D., Thiele, I., & Palsson, B. Ø. (2010). What is flux balance analysis? *Nature Biotechnology*, *28*, 245–248. https://doi.org/10.1038/nbt.1614

Parichehreh, R., Gheshlaghi, R., Mahdavia, M. A., & Elkamel, A. (2019). Optimization of lipid production in *Chlorella vulgaris* for biodiesel production using flux balance analysis. *Biochemical Engineering Journal*, *141*, 131–145. https://doi.org/10.1016/j.bej.2018.10.011

Paton, F. M., & Jennings, D. H. (1989). Evidence that *Thraustochytrium* is unable to synthesize lysine. *Mycological Research*, *92*, 470–476. https://doi.org/10.1016/S0953-7562(89)80193-5

Peppler, H. J. (1965). Amino acid composition of yeast grown on different spent sulfite liquors. *Journal of Agricultural and Food Chemistry*, *13*, 34–36.

Pike, I. H., & Jackson, A. (2010). Fish oil: Production and use now and in the future. *Lipid Technology*, *22*, 59–61. https://doi.org/10.1002/lite.201000003

Qiu, X., Hong, H., & MacKenzie, S. L. (2001). Identification of a Δ4 fatty acid desaturase from Thraustochytrium sp. involved in the biosynthesis of docosahexanoic acid by heterologous expression in *Saccharomyces cerevisiae* and *Brassica juncea*. *Journal of Biological Chemistry*, *276*, 31561–31566. https://doi.org/10.1074/jbc.M102971200

Quilodrán, B., Hinzpeter, I., Hormazabal, E., Quiroz, A., & Shene, C. (2010). Docosahexaenoic acid (C22: 6n-3, DHA) and astaxanthin production by a native *Ulkenia* strain: Evaluation of food industry liquid residues as nutrient sources. *Enzyme and Microbial Technology*, *47*, 24–30. https://doi.org/10.1016/j.enzmictec.2010.04.002

Santos, F., Boele, J., & Teusink, B. (2011). A practical guide to genome-scale metabolic models and their analysis. *Methods in Enzymology*, *500*, 509–532. https://doi.org/10.1016/B978-0-12-385118-5.00024-4

Schellenberger, J., Que, R., Fleming, R. M., Thiele, I., Orth, J. D., Feist, A. M., … Palsson, B. Ø. (2011). Quantitative prediction of cellular metabolism with constraint-based models: The COBRA Toolbox v2.0. *Nature Protocols*, *6*, 1290–1307. https://doi.org/10.1038/nprot.2011.308

Shene, C., Asenjo, J. A., & Chisti, Y. (2018). Metabolic modelling and simulation of the light and dark metabolism of *Chlamydomonas reinhardtii*. *The Plant Journal*, *96*, 1076–1088. https://doi.org/10.1111/tpj.14078

Shene, C., Leyton, A., Rubilar, M., Pinelo, M., Acevedo, F., & Morales, E. (2013). Production of lipids and docosahexaenoic acid by a native Thraustochytrium strain. *European Journal of Lipid Science and Technology*, *115*, 890–900. https://doi.org/10.1002/ejlt.201200417

Shene, C., Paredes, P., Vergara, D., Leyton, A., Garcés, M., Flores, L., … Armenta, R. (2019). Antarctic thraustochytrids: Producers of long chain omega-3 polyunsaturated fatty acids. *Microbiology Open*, *9*, e00950. https://doi.org/10.1002/mbo3.950

Singh, P., Liu, Y., Li, L., & Wang, G. (2014). Ecological dynamics and biotechnological implications of thraustochytrids from marine habitats. *Applied Microbiology and Biotechnology*, *98*, 5789–5805. https://doi.org/10.1007/s00253-014-5780-x

Sun, G. Y., Simonyi, A., Fritsche, K. L., Chuang, D. Y., Hannink, M., Gu, Z., … Beversdorf, D. Q. (2018). Docosahexaenoic acid (DHA): An essential nutrient and a nutraceutical for brain health and diseases. *Prostaglandins Leukotrienes and Essential Fatty Acids*, *136*, 3–13. https://doi.org/10.1016/j.plefa.2017.03.006

Ujihara, T., Nagano, M., Wada, H., & Mitsuhashi, S. (2014). Identification of a novel type of polyunsaturated fatty acid synthase involved in arachidonic acid biosynthesis. *FEBS Letters*, *588*, 4032–4036. https://doi.org/10.1016/j.febslet.2014.09.023

Valentine, R. C., & Valentine, D. L. (2004). Omega-3 fatty acids in cellular membranes: A unified concept. *Progress in Lipid Research*, *43*, 383–402. https://doi.org/10.1016/j.plipres.2004.05.004

Weiser, M. J., Butt, C. M., & Mohajeri, M. H. (2016). Docosahexaenoic acid and cognition throughout the lifespan. *Nutrients*, *8*, 99. https://doi.org/10.3390/nu8020099

Winwood, R. J. (2013). Recent developments in the commercial production of DHA and EPA rich oils from micro-algae. *Oilseeds and Fats, Crops and Lipids*, *20*, D604. https://doi.org/10.1051/ocl/2013030

Yaguchi, T., Tanaka, S., Yokochi, T., Nakahara, T., & Higashihara, T. (1997). Production of high yields of docosahexaenoic acid by *Schizochytrium* sp. strain SR21. *Journal of the American Oil Chemists' Society*, *74*(1431–1434), https://doi.org/10.1007/s11746-997-0249-z

Ye, C., Qiao, W., Yu, X., Ji, X., Huang, H., Collier, J. L., & Liu, L. (2015). Reconstruction and analysis of the genome-scale metabolic model of *Schizochytrium limacinum* SR21 for docosahexaenoic acid production. *BMC Genomics*, *16*, 799. https://doi.org/10.1186/s12864-015-2042-y

Yokoyama, R., & Honda, D. (2007). Taxonomic rearrangement of the genus *Schizochytrium* sensu lato based on morphology, chemotaxonomic characteristics, and 18S rRNA gene phylogeny (Thraustochytriaceae, Labyrinthulomycetes): Emendation for *Schizochytrium* and erection of *Aurantiochytrium* and *Oblongichytrium* gen. nov. *Mycoscience*, *48*, 199–211. https://doi.org/10.1007/S10267-006-0362-0

Zhang, L., Zhao, H., Lai, Y., Wu, J., & Chen, H. (2013). Improving docosahexaenoic acid productivity of *Schizochytrium* sp. by a two-stage AEMR/shake mixed culture mode. *Bioresource Technology*, *142*, 719–722. https://doi.org/10.1016/j.biortech.2013.05.072

SUPPORTING INFORMATION

Additional supporting information may be found online in the Supporting Information section.

How to cite this article: Shene C, Paredes P, Flores L, Leyton A, Asenjo JA, Chisti Y. Dynamic flux balance analysis of biomass and lipid production by Antarctic thraustochytrid *Oblongichytrium* sp. RT2316-13. *Biotechnology and Bioengineering*. 2020;1–12. https://doi.org/10.1002/bit.27463